Electronic stopping power of protons in platinum: Direct valence and inner-shell-electron excitations from first-principles calculations

Chang-Kai Li [1], Xun Guo,[2] Jian-Ming Xue,[1,*] and Feng-Shou Zhang [3,4,5]

[1]*State Key Laboratory of Nuclear Physics and Technology, School of Physics, Peking University, Beijing 100871, People's Republic of China*

[2]*Advanced Research Institute of Multidisciplinary Science, Beijing Institute of Technology, Beijing 100081, People's Republic of China*

[3]*The Key Laboratory of Beam Technology and Material Modification of Ministry of Education, College of Nuclear Science and Technology, Beijing Normal University Beijing 100875, China*

[4]*Beijing Radiation Center, Beijing 100875, China*

[5]*Center of Theoretical Nuclear Physics, National Laboratory of Heavy Ion Accelerator of Lanzhou, Lanzhou 730000, China*

The electronic energy loss of proton in platinum (Pt) is studied through nonadiabatic electron-ion coupling dynamic simulations within time-dependent density functional formalism. We have clarified the counterintuitive deviation from velocity proportionality due to the existence of kink velocity of the d electron excitation for a slow proton moving in metal Pt, whose valence d band indeed extends up above the Fermi energy. We have also quantitatively investigated the involvement of the host core electron excitation in the ion-target interaction, through monitoring the evolution of the bound electron number on a specific orbital of the host atom during the close encounter with the flying incident ion. It is found that the low-lying $5p$, $5s$, and $4f$ configuration excitations play significant roles in determining the profile of the stopping curve around and above the stopping maximum.

I. INTRODUCTION

The traverse of an energetic ion through matter is inevitably subject to energy dissipation in the interaction with target nuclei and electrons. When the charged particle is fast enough (typically greater than the host Fermi velocity v_F), the kinetic energy loss is mainly transferred to the electronic degree of freedom due to the extremely short interaction time and the significant difference in inertia between the nucleus and electron. The dissipative force thus generated is formally referred to as the electronic stopping power S_e, which is typically denoted as the rate of energy transfer from the charged particle to electrons in matter per unit distance of the intruding particle's movement.

Extensive efforts have been devoted to quantifying the electronic stopping and exploring the mechanism involved ever since the early days of ion physics [1–3]. Light incident ions such as the proton and helium ion are of special interest due to their simplicity in electronic configuration that allows one to concentrate on the underlying physical mechanism of excitations in the target material. Historically, a wide range of analytical models has been developed to predict electronic stopping with a varied degree of success. For the electronic stopping power of ions with relatively high particle energies, it can be well handled through the Bethe formula [3] and Lindhard-Winther theory [4]. At low ion velocities, the first-order approximation of Lindhard-Scharff theory [5] predicts that S_e is linearly proportional to the incident particle velocity. Another commonly used model with respect to the

electronic energy loss of slow ions, particularly with regard to metals, is the free-electron gas (FEG) by Fermi and Teller [6]. Under this formalism, S_e also falls in graceful velocity proportionality.

In systems such as the noble metals Cu, Ag, and Au, the electronic stopping power for slow light ions exhibits a pronounced deviation from velocity proportionality [7–14]. This effect was theoretically explained by the existence of finite thresholds for the excitation of d electrons due to a shift in the corresponding density of states of the d bands with respect to the Fermi energy E_F. For material with a d band extending up above E_F, such as Pd and Pt [15], it is expected to show no threshold effect for d-band excitation [16], and this has been verified by Celedón *et al.* for hydrogen ion in Pd [17]. However, the experimental data for the hydrogen ion in Pt by Goebl *et al.* [18] show some indications of a possible deviation from the velocity proportionality at velocities around 0.2 a.u., similar to the noble metals, although the reported effect is subject to the order of one standard deviation. They attributed such behavior to the difference in excitation efficiencies for d and s electrons. Later on, Celedón *et al.* [15] showed a significant deviation from the velocity proportionality at $v < 0.4$ a.u. in the measurement of S_e for a hydrogen ion transmitted through Pt.

Moreover, recent experimental data by Primetzhofer [19], Moro *et al.* [20], and Selau *et al.* [21] show contradictory results from the previous data for medium-energy ions (with velocity around the stopping maximum); and the electronic stopping power modeled by Peralta *et al.* [22] using the shellwise local plasma approximation (SLPA) and by Abril *et al.* [23] using the dielectric formalism agrees well with the recent experimental data around the stopping power

---

*Corresponding author: jmxue@pku.edu.cn

maximum. The theoretical results by Li *et al.* [24] suggest that the electronic stopping power for a proton transmitted through Pt is susceptible to the inner-shell configuration and impact parameter. In view of the above arguments, additional research is highly required to provide insight into this issue.

Over the past few decades, with the tremendous development of powerful computers and modern electronic structural methods, it has become possible to get key parameters such as the electron density and screened potential in analytical models directly from first-principles theories in a self-consistent way [25–27]. Such parameter-free methods have the potential to significantly go beyond analytical models, as they provide direct access to the coupling of ionic and electronic degrees of freedom, making it possible to study the nature of the electronic excitations during the ion-matter collision. In particular, the recent development of density functional theory (DFT) [28–33] explicitly takes into account the effects of inhomogeneity in electron density arising from the underlying lattice structure, band structure, and band gap, which are difficult to incorporate into analytical models.

In the early years when full *ab initio* calculations of electronic stopping were first developed, considerable effort was devoted to investigate electronic stopping at the low-velocity regime (below bohr velocity) [28,32,34–36], where electronic excitation comes from the weakly bound valence band. In recent years, it also appeared promising for obtaining stopping power curves even for higher ion velocities around and above the stopping maximum [33,37–43]; inner-shell-electron excitations hence have become relevant. However, due to the complexity in extracting the bound electron on a specific ionic shell orbital and, further, the ionic charge states directly from the electron density distribution, at present the inner-shell-electron excitation is mainly indirectly reflected as additional energy-loss channels beyond a certain velocity limit besides valence electron excitation. Direct access to the inner-shell-electron excitation and also the quantitative investigation of the threshold are highly desirable.

In this work, through time-dependent density functional theory (TDDFT) coupling Ehrenfest molecular dynamics (EMD) [44], we mainly address the counterintuitive departures from the velocity proportionality of S_e due to the existence of kink velocity for *d*-electron excitation during the movement of a proton in Pt. We also quantitatively investigate the contribution of the inner-shell electrons to the slowing down of the charged particle in solids over a wide range of velocities. The specific participation of the host core electrons in the ion-matter interaction is directly demonstrated through monitoring the inner-shell excitations during the close encounter between the incident ion and vicinal host atom.

This article is outlined as follows. In Sec. II, we briefly introduce the theoretical framework and the computational details. Results are presented and discussed in Sec. III, where we concentrate on the following two parts: we first discuss, in detail, the electronic stopping and *d*-band excitation in the low-velocity regime in Sec. III A, then we present the electronic stopping and the inner-shell excitation for a wide range of velocities in Sec. III B. Conclusions are drawn in Sec. IV.

II. MODEL AND METHODS

During the course of the simulation, the energy transferred to the host electronic system from the incident proton ion is monitored. For simplicity, and since the S_e is a velocity-resolved quantity, the intruder is constrained to move at a given velocity, hence the total energy of the system is not conserved. Therefore, instead of the decrease in projectile kinetic energy, the excess in total system energy is used in determining the key quantity electronic stopping. First, a ground-state DFT calculation is preformed to acquire the converged static state of the host Pt thin film. Then the initial bare intruding ions are implanted from a point that is 5 Å above the thin film, with the given descending velocities along the negative *z* direction. The ionic motion of target atoms is neglected by fixing them in the equilibrium positions as their velocity and movement are expected to undergo only a marginal change during the instantaneous interaction [45].

As the incident ion moves, the time-dependent Kohn-Sham (TDKS) equation describes the evolution of the electron density and energy of the system due to the dynamics of effective single-particle states under the external potential generated by the proton and host nuclei. These states evolve in time with a self-consistent Hamiltonian that is a function of the electron density $n(\vec{r}, t)$,

$$i\hbar \frac{\partial \varphi_i(\vec{r}, t)}{\partial t} = \left[-\frac{\hbar^2 \nabla^2}{2m} - V_{KS} \right] \varphi_i(\vec{r}, t), \quad (1)$$

with

$$V_{KS} = -\sum_I \frac{Z_I}{|\vec{R}_I(t) - \vec{r}|} + \int \frac{n(\vec{r}', t)}{|\vec{r} - \vec{r}'|} d\vec{r}' + V_{xc}(\vec{r}', t), \quad (2)$$

where Z_I and $\vec{R}_I(t)$ denote the charge and ionic position vector of the *I*th nucleus, respectively, *m* is the electron mass, and $\varphi_i(\vec{r}, t)$ is the orbital of the *i*th electron. V_{xc} is the time-dependent exchange-correlation potential; in the present work, the adiabatic local-density approximation with Perdew-Wang analytic parametrization [46] is employed. It is noted that V_{xc} is initially a function of electron density $n(\vec{r}', t')$ at all points $\vec{r}'$ and at all times $t' \leqslant t$. Since the adiabatic approximation is exploited in this work, any memory effects [47] of V_{xc} are neglected; as a result, V_{xc} is only a functional of instantaneous electron density $n(\vec{r}', t)$ at the current time *t*. Nazarov *et al.* [48] have shown that the error introduced by the adiabatic approximation is negligibly small for low-*Z* ions such as protons and α particles. The other two terms of V_{KS} are the electron-nucleus potential and the Hartree potential, respectively. The instantaneous electron density $n(\vec{r}, t)$ is obtained by summing all occupied individual electronic orbitals,

$$n(\vec{r}, t) = \sum_{i=1}^{occ} |\varphi_i(\vec{r}, t)|^2. \quad (3)$$

Theoretically, knowledge of the electron density distribution $n(\vec{r}, t)$ makes possible the quantitative determination of all the ionic charge states. However, it is difficult to determine the boundary of a specific atom when electron distributions from neighboring atoms are overlapped [49]. To circumvent the above-mentioned question, a space-free charge analysis

method through calculation of the projected density of states (PDOS) on a specific orbital is employed. We first calculate the PDOS on the specific orbital of the ion by projecting all single-orbital states of the system onto it,

$$\rho_j(\varepsilon) = \sum_i \langle \varphi_i | j \rangle \langle j | \varphi_i \rangle \delta(\varepsilon - \varepsilon_i). \qquad (4)$$

Energy integrating of the $\rho_j(\varepsilon)$ below the Fermi energy multiplied by the occupation number per state gives the number of bound electrons on a specific j orbital, whether it belongs to either the projectile or host atoms.

The simulations are carried out by using the OCTOPUS *ab initio* real-space code [50,51]. There is no basis set in such code; the external potential, electron density, and KS orbitals are discretized in a set of mesh grid points, and the spacing of the mesh grid corresponds to the energy cutoff in the plane-wave basis. In the present work, a uniform spacing of 0.18 Å along the three spatial coordinates is employed, which corresponds to an energy cutoff about 1160.59 eV in the plane-wave basis. A small time step of 0.001 fs is adopted to ensure the stability of the time-dependent computations. Simulations with smaller time steps and grid spacings give essentially the same results. To investigate the effect of inner-shell-electron excitation on S_e, three pseudopotentials, namely, Pt10 ([core]$^{68}5d^96s^1$), Pt18 ([core]$^{60}5s^25p^65d^96s^1$), and Pt32 ([core]$^{46}4f^{14}5s^25p^65d^96s^1$) with 10, 18, and 32 electrons explicitly included, are employed. The electrons frozen in the ionic core cannot polarize or take part in any dynamical process. As suggested by Grinberg *et al.* [52], for elements with $Z > 54$, relativistic effects should not be ignored. All the atoms, including the projectile proton in the present work, are represented by scalar-relativistic nonlocal pseudopotentials, factorized in the Kleinman-Bylander form [53].

Instead of converging a classical ensemble average of projectile trajectories, the "centroid trajectory" suggested in Refs. [38,43,54] is used to reduce the vast computational cost of TDDFT simulations. Such a channeling trajectory is often considered a good approximation to an ensemble average over all trajectories [38,43,54]. Thus, we have chosen the electronic stopping power along this trajectory to represent the electronic energy-loss rate during the collisions. The host crystalline thin film is an isolate atom cluster; no periodic boundary condition is employed in this work. To allow time for the intruding ion to get fully equilibrated during passage through the crystal, a relatively thick face-centered-cubic structural 2×2×4 conventional cell comprising 64 Pt atoms is employed. The lattice parameter exploited in this work is 3.92 Å, identical to the experimental value [55].

III. RESULTS AND DISCUSSION

A. Characteristic of *d*-band excitation on stopping in low-velocity regime

Figure 1 shows the increase of the system total energy as a function of projectile displacement along the centroid trajectory in the ⟨100⟩ channel for a proton with velocity 1.0 a.u. In the present work, the calculated S_e data are extracted by linear fitting of the increase in system energy over the ion path covering the last four lattice layers with length
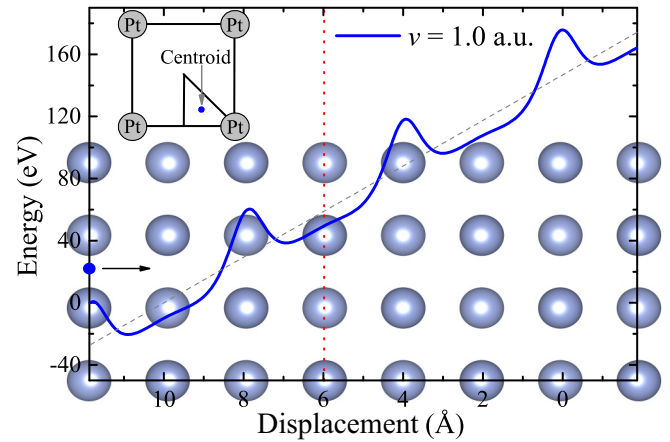

FIG. 1. Increase of system total energy as a function of projectile displacement along the centroid trajectory in the ⟨100⟩ channel, which is parallel to the *z* axis, for a proton with velocity 1.0 a.u. (solid blue line). The gray dashed line is the linear fit of the curve. The black arrow line denotes the movement direction of the irradiating ion. In the present work, only the increase of the system total energy in the ion path (on the right side of the vertical red dotted line) is employed to extract S_e. The upper inset shows the sketch of the centroid trajectory; the lower inset shows the positions of the Pt lattice layers along the *z* axis.

of 7.84 Å in conducting solids to minimize the preequilibrium contributions [49] to the stopping.

We present, in Fig. 2, the simulated S_e results for the motion of the proton with velocity of 0.1–0.6 a.u. along the centroid trajectory in the ⟨100⟩ channel of the Pt thin film. Also shown are the experimental data by Goebl *et al.* [18] and Celedón *et al.* [15]. Since electronic excitation in such
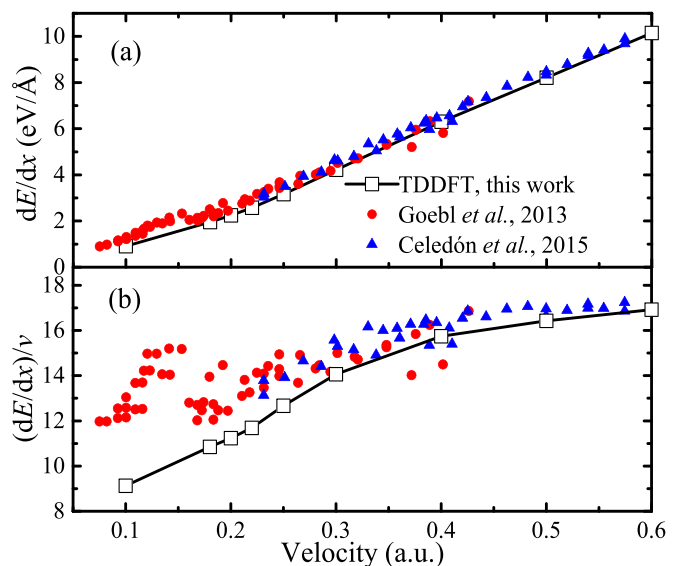

FIG. 2. (a) Electronic stopping power (black open squares) for channeled protons as a function of velocity along the centroid trajectory in the ⟨100⟩ channel, together with experimental data (solid symbols) by Goebl *et al.* [18] and Celedón *et al.* [15]. (b) The electronic stopping power in (a) scaled by velocity as a function of velocity.
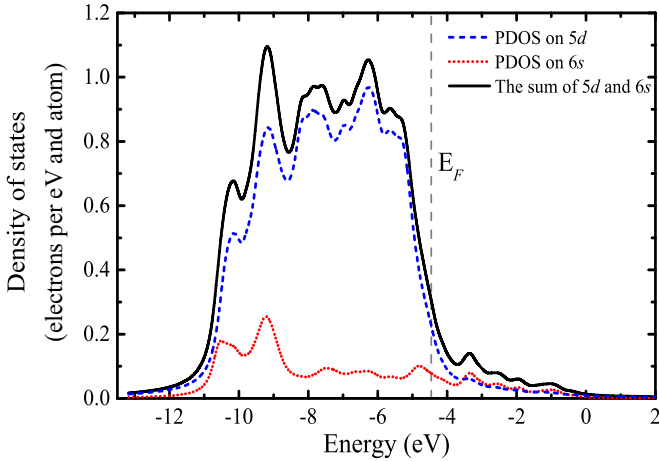
FIG. 3. Projected density of states on $5d$ and $6s$ orbitals and also the sum of the two; the amplitude has been scaled by atoms number. The vertical gray dashed line denotes the position of the Fermi energy.
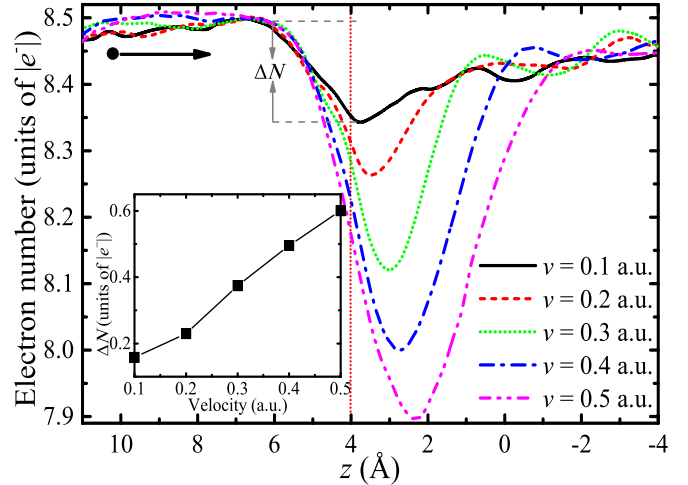

FIG. 4. Evolution of $5d$ bound electron on Pt atom positing at the lower right corner of the upper inset in Fig. 1 with the position of the incident ion. The red vertical dotted line shows the position of the researched Pt atom; the black arrow shows ion movement direction. The inset shows the velocity-resolved number of excited $5d$ electrons ΔN during close ion-target encounter; it is the discrepancy of the instantaneous $5d$ electron number on the researched Pt atom between when the excitation begins to occur and the maximum extent at the curve valley (see the schematic of ΔN for $v = 0.1$ a.u.). It can be seen that for nearly all the velocities, the excitations begin to occur when the oncoming projectile moves to 2 Å perpendicular distance from the researched Pt atom.

low-velocity regime induced by the channeled light ion mainly arises from the valence band [9,40], the Pt10 pseudopotential with nine $5d$ electrons and one $6s$ electron explicitly considered is employed. It can be seen in Fig. 2(a) that the calculated results are in excellent agreement with the experimental data and the kink velocity at 0.2 a.u. reported by Goebl *et al.* [18] is reproduced, indicating that the centroid trajectory approximation is quite valid for the considered low-velocity regime. In order to highlight the kink in S_e, we present, in Fig. 2(b), the velocity scaled S_e as a function of velocity. It exhibits a pronounced increase for transition from a relatively low-velocity to higher-velocity regime around $v = 0.2$ a.u.; the value of $v = 0.3$ a.u. is about 50% higher than that of $v = 0.1$ a.u.

To illustrate the electronic property of Pt10, we show, in Fig. 3, the projected density of states on $5d$ and $6s$ orbitals and also the sum of the two, respectively. As can be seen, the main part of the $5d$ component has a wide distribution about 8 eV, and the high-energy edge extends above the E_F. Thus no threshold in the $5d$ electron excitation is expected according to the interpretation in Ref. [16]. For the $6s$ components, its main distributions are much lower than E_F, and the amplitude of PDOS on the $6s$ orbital is significantly lower than that on the $5d$ orbital around E_F. Thus, $5d$ excitation is expected to play a major role in the interaction with a slow ion. In order to explore the d-electron excitation in the low-velocity regime, we monitor the evolution of $5d$ bound electrons on Pt atom positing at $z = 4.02$ Å of the host atom's string closest to the projectile trajectory (the Pt atom positing at the lower right corner of the upper inset in Fig. 1), during the ion passage through the host thin film. The results are demonstrated in Fig. 4. It is conspicuous that the $5d$ bound electron number is less than 9 and no excitation threshold for the $5d$ electron as low as $v = 0.1$ a.u. is found; these can be attributed to the electronic structure characteristic that part of the $5d$ band distributes above E_F. Particularly noteworthy is that the electronic excitation is quite a local event; it begins to occur when incident protons reach as close as about 2 Å

perpendicular distance from the target Pt atom. The durations of the electronic excitation depend on the impact velocity, and the maximum extents that show as global valleys in electron number curves with varied amplitudes are reached.

We note that the excitation mainly occurs at the oncoming collision phase. This can be qualitatively rationalized by the inhomogeneity in the electronic screening effect due to the wake potential [16,56–58], where the electrons are more concentrated in the back of the flying ion, leading to the unbalanced electronic screening in the front and the back of the flying ion. This effect is particularly obvious in the very low-velocity region: for a proton with velocity of 0.1 a.u., nearly all the excitations occur at the oncoming collision phase. As the impact of the velocities increases, there is a significant increase in excitation during the departure phase, which results in enhanced d-electron excitation, as shown in the inset of Fig. 4. Thus we interpret that the change of the stopping curve slope around 0.2 a.u. in Fig. 2 mainly comes from the change in d-electron excitation efficiency that is closely related to the impact velocity, probably due to charge states of the projectile which we will demonstrate in the following section.

B. Stopping of projectiles including inner-shell-electron excitation

In order to investigate the involvement of inner-shell excitation in electronic stopping, we extend the impact velocity to 6.0 a.u. The calculated results together with experimental data by Krist and Mertens [59,60], Sirotinin *et al.* [61], Goebl *et al.* [18], Celedón *et al.* [15], Primetzhofer [19], Moro
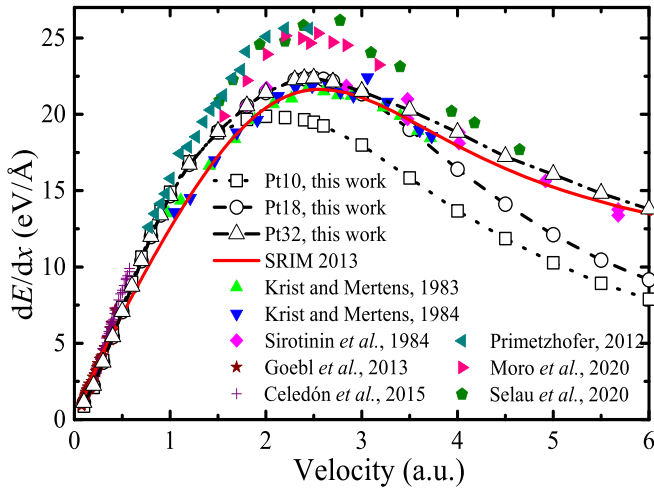
FIG. 5. Electronic stopping power (black open squares, circles, and upper triangle) for channeled protons as a function of velocity along the centroid trajectory in the ⟨100⟩ channel, together with the SRIM-2013 predictions (solid line) and the experimental data (solid symbols) by Krist and Mertens [59,60], Sirotinin *et al.* [61], Goebl *et al.* [18], Celedón *et al.* [15], Primetzhofer [19], Moro *et al.* [20], and Selau *et al.* [21].
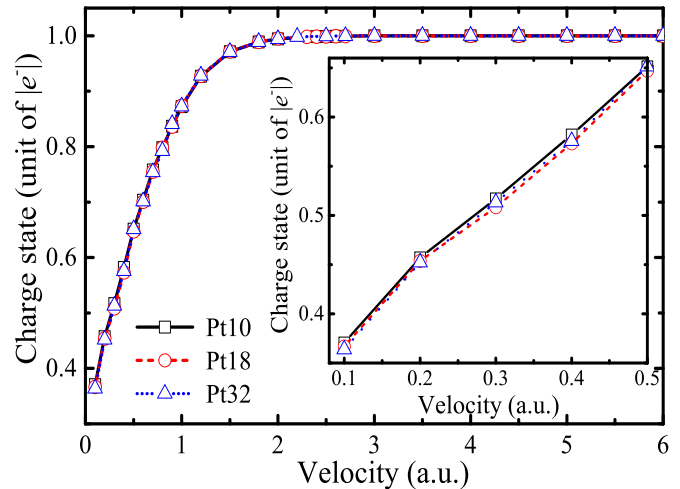

FIG. 6. Velocity-resolved effective charge state for a proton in Pt10, Pt18, and Pt32, respectively. The inset shows the amplification of the low-velocity regime.

et al. [20], and Selau *et al.* [21], as well as the SRIM-2013 predictions, are presented in Fig. 5. As can be seen, the calculated S_e for Pt10 saturates at lower velocity and the amplitude of the maximum value underestimates the SRIM data by about 15%. Such situation is improved by including the $5s$ and $5p$ configurations. For a proton interacting with Pt18, both the position and amplitude of the stopping maximum match well with the SRIM data. However, in a velocity regime above 3.5 a.u., the calculated results for Pt18 also underestimate the SRIM data (the simulated result is about 20% lower than the SRIM data at $v = 5.0$ a.u.), indicating that more inner-shell configurations should be included in the high-velocity regime. Furthermore, we calculate S_e for a proton in Pt32 with 14 additional $4f$ electrons explicitly included. As shown in Fig. 5, the agreement with the SRIM data for the calculated results is significantly improved in the high-velocity regime ($v \geqslant 3$ a.u.).

It is noted that our calculated data, which generally agree well with the SRIM data, obviously underestimate the recent experimental data by Primetzhofer [19], Moro *et al.* [20], and Selau *et al.* [21] around the stopping maximum. Such results can be attributed to the channeling centroid path approximation employed in this work since, along this path, the proton projectile does not come near the host Pt atoms, which possibly omits the strong interaction with tightly bound inner-shell electrons. As reported by Li *et al.* [24], such condition can be improved with a random trajectory considered.

Although including inner-shell configurations means opening additional electronic excitation channels in the target, which indeed improve the calculation especially in the high-velocity regime, one should also keep in mind that the projectile charge state, which is possibly susceptible to the inclusion of inner-shell electrons, also plays a significant role in determining the electronic stopping.

To explore the possible difference introduced by the screening effect from the bound electron on the projectile,

we calculated the effective charge states (atomic number minus the bound electron number) of incident protons during the interaction with Pt10, Pt18, and Pt32, respectively. The bound electron number of incident protons is derived by averaging the electron on the $1s$ orbital of a proton over the ion path covering the last four lattice layers with length 7.84 Å in conducting solids. The effective charges as a function of velocity are presented in Fig. 6. As can be seen, for interactions with Pt10, Pt18, and Pt32, the number of $1s$ bound electrons on the proton decreases rapidly with velocity for a velocity regime below 1.5 a.u., and reaches fully deprived states at about 2.0 a.u. Only a very slight difference can be found for the charge state of the proton in Pt10, Pt18, and Pt32 in the low-velocity regime of $v \leqslant 0.5$ a.u. The divergence diminishes at higher velocities, indicating that host inner-shell configurations have a minor influence on the charge state of the light proton projectile, and the increased S_e for a proton in Pt32 and Pt18 with respect to Pt10 mainly comes from additional inner-shell excitations.

Now let us return to the change of d-electron excitations in low velocity shown in the inset of Fig. 4. As can be seen in the inset of Fig. 6, there is a pronounced kink point in the slope of the curve for charge states at $v = 0.2$ a.u., and the reduction in charge states is steeper below $v = 0.2$ a.u. As we know, a low charge state means high electronic screening from bound electrons; it thus can be inferred that the change in the impact velocity-dependent excitation duration stems from the change of electronic state of the projectile.

Excluding the influence factor of incident ions, we conclude that the main discrepancy in electronic stopping for a proton in Pt10, Pt18, and Pt32 comes from the target's low-lying $5p$, $5s$, and $4f$ band excitation. We present, in Fig. 7, the excitation of $5p$ and $5s$ electrons for a proton in Pt18, and the $4f$ band excitation for a proton in Pt32. As can be seen in Fig. 7, for velocities below 0.8 a.u., no excitation in $5p$ electrons can be observed. When the impact velocity increases to 1.2 a.u., the $5p$ electrons' excitation becomes evident. Thereafter, the excitation increases significantly with velocity and
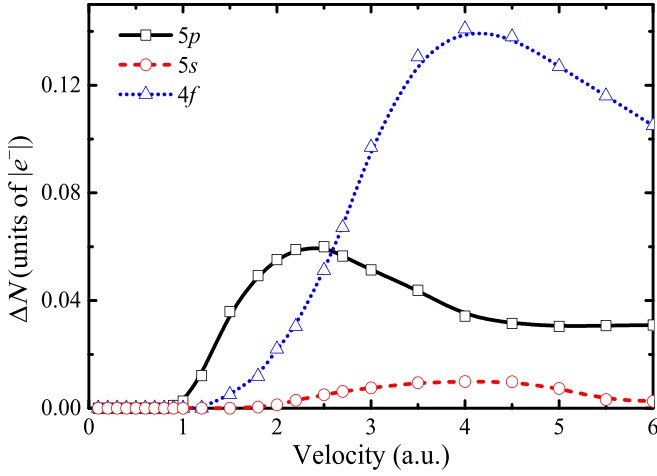
FIG. 7. Velocity-resolved 5*p*, 5*s*, and 4*f* electron excitations during close ion-target encounter. The number of excited electrons, Δ*N*, is the discrepancy of the instantaneous electron number on a specific orbital of the researched Pt atom between when the excitation begins to occur and the maximum extent at the curve valley (see the schematic in Fig. 4 for a more detailed introduction of the derivation of Δ*N*).

reaches its maximum at about $v = 2.5$ a.u., which corresponds to the velocity of the stopping maximum for a proton in Pt18 shown in Fig. 5, suggesting that the 5*p* electrons' excitation plays a significant role around the stopping maximum. The excitation of 5*s* and 4*f* electrons demonstrates a similar profile as that of 5*p* electrons; there are thresholds at $v = 2.0$ and 1.2 a.u. and maximum excitation intensity at $v = 4.5$ and 4.2 a.u., respectively. It is noted that the major excitation regime of 4*f* electrons (around $v = 4$ a.u.) overlaps with the region where S_e for a proton in Pt18 underestimates the experimental data, confirming such underestimation is due to neglecting 4*f* electron excitations. For the 5*p*, 5*s*, and 4*f* cases, the excitations decrease monotonically after the maximum. It is somewhat counterintuitive since the higher impact velocity means more powerful ionization capability. The explanation for this is that the maximum of excitation as a function of velocity is a compromise of excitation capability and interaction time, in which the former is positively related with the projectile charge state and also impact velocity [62]. Beyond the critical value (typically close to the mean electron velocity of the specific shell) [63], the decrement in interaction time due to the increase of velocity plays a more significant role.

We also calculated the threshold of the impact velocity for the excitation of 5*p*, 5*s*, and 4*f* electrons of Pt through the method suggested by Lim *et al.* [31] and Lee *et al.* [40]. The channeling of the projectile through a periodic lattice is viewed as time-dependent perturbation to the target material. The energy is quantified as $\hbar\omega$, with $\omega = 2\pi v/\lambda$, where λ

is the distance between equivalent lattice positions (for the ⟨100⟩ channel of Pt crystal, $\lambda = a/2$, where a is the lattice parameter). The threshold velocity v_{th} can be obtained by equating perturbation $\hbar\omega$ to the binding energy ΔE, giving

$$v_{th} = \frac{\lambda \Delta E}{h}, \tag{5}$$

where h is Planck's constant. We estimate that for the 5*p*, 4*f*, and 5*s* electrons of Pt with binding energy about 52, 71, and 101 eV [64], respectively, it only contributes to electronic stopping for a projectile with velocities above 1.15, 1.57, and 2.2 a.u., slightly overestimating the thresholds 0.8, 1.2, and 2.0 a.u. predicted by the TDDFT results.

IV. CONCLUSIONS

We report a theoretical study from first principles of the nonadiabatic interaction of a proton with Pt in a wide range of velocities along the centroid trajectory. There is generally good agreement between the calculated results and the experimental data all through the velocity regime considered here. Deviation of electronic stopping from the velocity proportionality is found in the low-velocity regime and is ascribed to the change of charge-state-dependent *d*-band excitation efficiency around the kink velocity. During the quantitative demonstration of the *d*-band excitation, the localized property is unveiled.

Furthermore, we find that the electronic stopping is significantly underestimated in the velocity regime around and above the stopping maximum with target inner-shell configurations frozen. The results are improved when core electrons are incorporated, indicating that inner-shell excitations play a significant role in determining the amplitude of the stopping curve around and above the stopping maximum. In addition, it is found that host inner-shell configurations have a minor influence on the charge state of the light projectile proton. Furthermore, we demonstrate quantitatively the inner-shell excitation during the process of projectile encountering with vicinal host atoms; the trend of inner-shell excitation is consistent with that of electronic stopping. The charge analysis method in this work makes possible direct access to the electronic excitation on a specific electronic orbital, which provides insight into the study of electron excitation in ion-matter interaction.

[1] E. Rutherford, London, Edinburgh Dublin Philos. Mag. J. Sci. **21**, 669 (1911).

[2] N. Bohr, London, Edinburgh Dublin Philos. Mag. J. Sci. **30**, 581 (1915).

[3] H. Bethe, Ann. Phys. **397**, 325 (1930).

[4] J. Lindhard and A. Winther, K. Dan. Vidensk. Selsk. Mat. Fys. Medd. **34**, No. 4 (1964).

[5] J. Lindhard and M. Scharff, Phys. Rev. **124**, 128 (1961).

[6] E. Fermi and E. Teller, Phys. Rev. **72**, 399 (1947).

[7] J. E. Valdés, G. A. Tamayo, G. H. Lantschner, J. C. Eckardt, and N. R. Arista, Nucl. Instrum. Methods Phys. Res. Sec. B **73**, 313 (1993).

[8] J. E. Valdés, J. C. Eckardt, G. H. Lantschner, and N. R. Arista, Phys. Rev. A **49**, 1083 (1994).

[9] M. A. Zeb, J. Kohanoff, D. Sánchez-Portal, A. Arnau, J. I. Juaristi, and E. Artacho, Phys. Rev. Lett. **108**, 225504 (2012).

[10] S. N. Markin, D. Primetzhofer, M. Spitz, and P. Bauer, Phys. Rev. B **80**, 205105 (2009).

[11] E. A. Figueroa, E. D. Cantero, J. C. Eckardt, G. H. Lantschner, J. E. Valdés, and N. R. Arista, Phys. Rev. A **75**, 010901(R) (2007).

[12] E. D. Cantero, G. H. Lantschner, J. C. Eckardt, and N. R. Arista, Phys. Rev. A **80**, 032904 (2009).

[13] S. N. Markin, D. Primetzhofer, S. Prusa, M. Brunmayr, G. Kowarik, F. Aumayr, and P. Bauer, Phys. Rev. B **78**, 195122 (2008).

[14] G. Martínez-Tamayo, J. C. Eckardt, G. H. Lantschner, and N. R. Arista, Phys. Rev. A **54**, 3131 (1996).

[15] C. Celedón, E. Sánchez, L. S. Alarcón, J. Guimpel, A. Cortés, P. Vargas, and N. R. Arista, Nucl. Instrum. Methods Phys. Res. Sec. B **360**, 103 (2015).

[16] E. E. Quashie, B. C. Saha, and A. A. Correa, Phys. Rev. B **94**, 155403 (2016).

[17] C. Celedón, E. A. Sánchez, M. S. Moreno, N. R. Arista, J. D. Uribe, M. Mery, J. E. Valdés, and P. Vargas, Phys. Rev. A **88**, 012903 (2013).

[18] D. Goebl, D. Roth, and P. Bauer, Phys. Rev. A **87**, 062903 (2013).

[19] D. Primetzhofer, Phys. Rev. B **86**, 094102 (2012).

[20] M. V. Moro, P. Bauer, and D. Primetzhofer, Phys. Rev. A **102**, 022808 (2020).

[21] F. F. Selau, H. Trombini, G. G. Marmitt, A. M. H. de Andrade, J. Morais, P. L. Grande, I. Alencar, M. Vos, and R. Heller, Phys. Rev. A **102**, 032812 (2020).

[22] J. P. Peralta, M. Fiori, A. M. P. Mendez, and C. C. Montanari, Phys. Rev. A **105**, 062814 (2022).

[23] I. Abril, P. de Vera, and R. Garcia-Molina, J. Phys.: Conf. Ser. **2326**, 012016 (2022).

[24] S.-M. Li, F. Mao, X.-D. Zhao, W.-Q. Jin, W.-Q. Zuo, B.-S. Li, F. Wang, and F.-S. Zhang, Phys. Rev. B **106**, 014103 (2022).

[25] P. M. Echenique, R. M. Nieminen, J. C. Ashley, and R. H. Ritchie, Phys. Rev. A **33**, 897 (1986).

[26] A. Arnau, M. Peñalba, P. M. Echenique, F. Flores, and R. H. Ritchie, Phys. Rev. Lett. **65**, 1024 (1990).

[27] E. K. U. Gross and W. Kohn, Phys. Rev. Lett. **55**, 2850 (1985).

[28] R. Ullah, F. Corsetti, D. Sánchez-Portal, and E. Artacho, Phys. Rev. B **91**, 125203 (2015).

[29] M. Caro, A. Tamm, A. Correa, and A. Caro, J. Nucl. Mater. **507**, 258 (2018).

[30] C.-K. Li, S. Liu, Q. Cao, F. Wang, X.-P. OuYang, and F.-S. Zhang, Phys. Rev. A **100**, 052707 (2019).

[31] A. Lim, W. M. C. Foulkes, A. P. Horsfield, D. R. Mason, A. Schleife, E. W. Draeger, and A. A. Correa, Phys. Rev. Lett. **116**, 043201 (2016).

[32] J. M. Pruneda, D. Sánchez-Portal, A. Arnau, J. I. Juaristi, and E. Artacho, Phys. Rev. Lett. **99**, 235501 (2007).

[33] R. Ullah, E. Artacho, and A. A. Correa, Phys. Rev. Lett. **121**, 116401 (2018).

[34] F. Mao, C. Zhang, J. Dai, and F.-S. Zhang, Phys. Rev. A **89**, 022707 (2014).

[35] C.-K. Li, F. Wang, B. Liao, X.-P. OuYang, and F.-S. Zhang, Phys. Rev. B **96**, 094301 (2017).

[36] C.-K. Li, F. Mao, F. Wang, Y.-L. Fu, X.-P. Ouyang, and F.-S. Zhang, Phys. Rev. A **95**, 052706 (2017).

[37] A. A. Shukri, F. Bruneval, and L. Reining, Phys. Rev. B **93**, 035128 (2016).

[38] D. C. Yost, Y. Yao, and Y. Kanai, Phys. Rev. B **96**, 115134 (2017).

[39] Y. Yao, D. C. Yost, and Y. Kanai, Phys. Rev. Lett. **123**, 066401 (2019).

[40] C.-W. Lee, J. A. Stewart, R. Dingreville, S. M. Foiles, and A. Schleife, Phys. Rev. B **102**, 024107 (2020).

[41] K. G. Reeves, Y. Yao, and Y. Kanai, Phys. Rev. B **94**, 041108(R) (2016).

[42] A. Schleife, Y. Kanai, and A. A. Correa, Phys. Rev. B **91**, 014306 (2015).

[43] A. Ojanperä, A. V. Krasheninnikov, and M. Puska, Phys. Rev. B **89**, 035120 (2014).

[44] X. Andrade, A. Castro, D. Zueco, J. L. Alonso, P. Echenique, F. Falceto, and A. Rubio, J. Chem. Theory Comput. **5**, 728 (2009).

[45] A. A. Correa, J. Kohanoff, E. Artacho, D. Sánchez-Portal, and A. Caro, Phys. Rev. Lett. **108**, 213201 (2012).

[46] J. P. Perdew and Y. Wang, Phys. Rev. B **45**, 13244 (1992).

[47] N. T. Maitra, K. Burke, and C. Woodward, Phys. Rev. Lett. **89**, 023002 (2002).

[48] V. U. Nazarov, J. M. Pitarke, Y. Takada, G. Vignale, and Y.-C. Chang, Phys. Rev. B **76**, 205103 (2007).

[49] A. Kononov and A. Schleife, Phys. Rev. B **102**, 165401 (2020).

[50] M. A. L. Marques, A. Castro, G. F. Bertsch, and A. Rubio, Comput. Phys. Commun. **151**, 60 (2003).

[51] A. Castro, H. Appel, M. Oliveira, C. A. Rozzi, X. Andrade, F. Lorenzen, M. A. L. Marques, E. K. U. Gross, and A. Rubio, Phys. Stat. Solidi B **243**, 2465 (2006).

[52] I. Grinberg, N. J. Ramer, and A. M. Rappe, Phys. Rev. B **62**, 2311 (2000).

[53] L. Kleinman and D. M. Bylander, Phys. Rev. Lett. **48**, 1425 (1982).

[54] A. Kononov and A. Schleife, Nano Lett. **21**, 4816 (2021).

[55] R. W. Wyckoff, Cryst. Struct. **1**, 7 (1963).

[56] P. M. Echenique, F. Flores, and R. H. Ritchie, in *Solid State Physics*, edited by H. Ehrenreich and D. Turnbull (Academic Press, Cambridge, MA, 1990), pp. 229–308.

[57] F. Matias, R. C. Fadanelli, P. L. Grande, N. R. Arista, N. E. Koval, and G. Schiwietz, Phys. Rev. A **98**, 062716 (2018).

[58] M. Quijada, A. G. Borisov, I. Nagy, R. Diez Muiño, and P. M. Echenique, Phys. Rev. A **75**, 042902 (2007).

[59] T. Krist and P. Mertens, Nucl. Instrum. Methods Phys. Res. Sect. B **218**, 790 (1983).

[60] T. Krist and P. Mertens, Nucl. Instrum. Methods Phys. Res. Sect. B **218**, 821 (1983).

[61] E. Sirotinin, A. Tulinov, V. Khodyrev, and V. Mizgulin, Nucl. Instrum. Methods Phys. Res. Sect. B **4**, 337 (1984).

[62] C.-K. Li, J.-M. Xue, and F.-S. Zhang, Phys. Rev. A **106**, 022807 (2022).

[63] R. A. Lewis, G. A. Smith, and W. S. Toothacker, Phys. Rev. A **44**, 392 (1991).

[64] G. P. Williams, http://xdb.lbl.gov/Section1/Sec_1-1.html.